A compact formulation for the retrieval of the overlap function in an elastic/Raman aerosol lidar

Adolfo Comerón[1], Constantino Muñoz-Porcar[1], Alejandro Rodríguez-Gómez[1], Michaël Sicard[1,2], Federico Dios[1], Cristina Gil-Díaz[1], Daniel Camilo Fortunato dos Santos Oliveira[1], Francesc Rocadenbosch[1,2]

[1]CommSensLab-UPC, Universitat Politècnica de Catalunya, 08034 Barcelona, Spain.

[2]Laboratoire de l'Atmosphère et des Cyclones (LACy), Université de la Réunion, Saint-Denis, France.

Correspondence to: Alejandro Rodríguez-Gómez (alejandro.rodriguez.gomez@upc.edu)

Abstract. We derive an explicit (i.e. non-iterative) formula for the retrieval of the overlap function in an aerosol lidar with both elastic and Raman N_2 or/and O_2 channels used for independent measurements of aerosol backscatter and extinction coefficients. The formula requires only the measured, range-corrected, elastic and the corresponding Raman signals, plus an assumed lidar ratio. We assess the influence of the lidar ratio error in the overlap function retrieval and present retrieval examples.

1. Introduction

At near ranges, lidar signals suffer from a varying overlap between the emitted laser beam and the field of view of the receiving optical assembly. The overlap function of a lidar system can be defined as the ratio between the power scattered by a scattering volume at a given range that reaches the photodetector (excluding transmission losses) and the power scattered by the same scattering volume that reaches the telescope aperture (Comeron et al., 2011). This ratio is a function of range, especially at short ranges, and depends on the optical and geometrical arrangement of the transmitting and receiving optics of the instrument. The key parameters determining the overlap function are those related to the laser beam features (diameter, shape and divergence), to the receiver optical properties (telescope diameter, focal length and field stop diameter) and to the relative location and alignment between transmitter and receiver optical axes (Halldórsson and Langerholc, 1978; Lefrère, 1982). In a perfectly aligned system, the overlap function is zero at the telescope aperture level and progressively grows up to a constant value, where all the backscattered radiation collected by the telescope aperture, or at least a constant proportion of it, reaches the photodetector. In practical cases, misalignments may make the overlap function dependence on range depart from the ideal behavior just described.

The existence of a varying overlap prevents the system to provide trustfully lidar signals for ranges below the altitude at which the overlap attains a constant value, thus limiting the minimum operational range of the lidar instrument. To reduce these overlap issues, some systems duplicate their receivers, enabling both far- and near-range telescopes and detectors, and combining their respective signals for reconstructing a lidar signal with an extended (towards the lower end) constant overlap range. For example, Polly[XT] systems (Engelmann et al., 2016) use this type of solution and their full overlap altitude is reduced down to ~100 m. Alternatives when such a hardware-based extension of the operational range is not possible rely on the calculation or estimation of the overlap function and on the correction of the detected signals from the effect of the varying overlap. Several authors have developed theoretical calculations of the overlap function using the transmitter and the receiver optical parameters, both on an analytical basis (Sassen and Dodd, 1982; Ancellet et al., 1986; Kuze et al., 1998; Stelmaszczyk et al., 2005; Comeron et al., 2011) and relying on ray tracing procedures (e.g. (Kumar and Rocadenbosch, 2013)). However, such theoretical approaches are in many cases not practical because most of the system parameters in which they are based on are not easily measurable (Kokkalis, 2017) and they change, sometimes unpredictably and unnoticeably, with time. Alternatives to theoretical calculations are based on experimental estimations relying on practical field lidar measurements and inversions. A first proposal, presented by Sasano et al in 1978 (Sasano et al., 1979), is based on the assumption of a homogeneous atmosphere up to distances above the full overlap altitude. In many cases, this method is not practical, first, because its applicability depends on the state of the atmosphere and second, because in order to assure the required atmospheric homogeneity, it demands for a horizontal alignment of the lidar line-of-sight that is not always possible. Further contributions, making different assumptions on the atmospheric conditions were proposed by (Tomine et al., 1989; Dho et al., 1997; Vande Hey et al., 2011).

A comparison with a reference system not affected (or less affected) by the varying overlap has been proposed by (Guerrero-Rascado et al., 2010). Other authors have proposed comparisons between Raman signals with radiosonde

profiles (Hu et al., 2005), nonlinear regression using optical analysis combined with measured aerosol optical thickness (Povey et al., 2012), as a by-product of a retrieval of temperature profiles with multiple pure rotational Raman channels, using an optimal estimation method (Mahagammulla Gamage et al., 2019). For motor-controlled lidars, a beam mapping procedure has been proposed by (Di Paolantonio et al., 2022).

Up to date, one of the best-established and widely accepted methods was presented by Wandinger and Ansmann (Wandinger and Ansmann, 2002). This approach assumes that the lidar system has a Raman channel to independently retrieve the aerosol extinction coefficient and relies on the fact that, under the assumption of the same overlap function for the elastic and the Raman channels, the Raman inversion of the backscatter coefficient is not affected by the incomplete overlap. Further contributions, including an analysis of the effect of the lidar ratio used, were reported by (Li et al., 2016).

In this paper, we present an alternative formulation for the retrieval of the overlap function based on the same principles as the one discussed in (Wandinger and Ansmann, 2002), i.e. the fact that the backscatter coefficient retrieved by the Raman method is not affected by the incomplete overlap. However, unlike in the Wandinger and Ansmann method, our formulation results in an explicit formula that does not require iterative inversions of the backscatter coefficient by both the Raman (Ansmann et al., 1992) and Klett (Klett, 1985; Sasano et al., 1985) methods. Section 2 develops the proposed formulation. In section 3 we assess the effect of an erroneous lidar ratio on the retrieved overlap function. Examples based on real measurements are presented in section 4. Conclusions and outlook are summed up in section 5.

2. Overlap retrieval

The proposed method uses, like ref. (Wandinger and Ansmann, 2002), the elastic and the Raman signals backscattered by an air volume under the excitation of one of the emitted wavelengths of an aerosol lidar. First, let's consider the expression of the range-corrected elastic lidar signal , $X(R)$, affected by an overlap function, $O(R)$, R being the range to the lidar, where the aerosol and molecular components of the extinction coefficient are written using the corresponding lidar ratios at the elastic wavelength, $S_{a0}(R)$ and S_{m0} (Bucholtz, 1995; D'Amico et al., 2016) respectively:

$$X(R) = A\, O(R)\left[\beta_{a0}(R) + \beta_{m0}(R)\right]\exp\left\{-2\int_0^R \left[S_{a0}(x)\beta_{a0}(x) + S_{m0}\beta_{m0}(x)\right]dx\right\}, \qquad (1)$$

where A is an instrument constant, and $\beta_{a0}(R)$ and $\beta_{m0}(R)$ are respectively the aerosol and molecular components of the backscatter coefficient at the emitted wavelength λ_0. To avoid using the instrument constant, we look for an aerosol-free range, R_m, at which the aerosol backscatter coefficient can be assumed to be zero and where $\beta_{m0}(R_m)$ can be estimated from the pressure and the temperature provided by a radiosonde or by using a standard model of the atmosphere. We assume as well that at that range the overlap function has attained a constant value that we set conventionally to $O(R_m) = 1$; we have at that range

$$X(R_m) = A\beta_{m0}(R_m)\exp\left\{-2\int_0^{R_m}\left[S_{a0}(x)\beta_{a0}(x) + S_{m0}\beta_{mo}(x)\right]dx\right\} \qquad (2)$$

Dividing Eq. (1) by Eq. (2) and re-ordering terms, we obtain:

$$O(R)\left[\beta_{a0}(R) + \beta_{m0}(R)\right]\exp\left[-2\int_{R_m}^R S_{a0}(x)\beta_{a0}(x)dx\right] = \beta_{m0}(R_m)\frac{X(R)}{X(R_m)}\exp\left[2S_{m0}\int_{R_m}^R \beta_{m0}(x)dx\right]. \qquad (3)$$

Now we follow steps similar to those leading to the well-known Klett's formula (Klett, 1985; Gimmestad and Roberts, 2010), but keeping explicitly the overlap function in the equations. Multiplying both members of Eq. (3) by $S_{a0}(R)\exp\left[-2\int_{R_m}^R S_{a0}(x)\beta_{m0}(x)dx\right]$, we obtain

$$O(R)S_{a0}(R)\left[\beta_{m0}(R) + \beta_{a0}(R)\right]\exp\left\{-2\int_{R_m}^R S_{a0}(x)\left[\beta_{a0}(x) + \beta_{m0}(x)\right]dx\right\} =$$

$$= \beta_{m0}(R_m)\frac{X(R)S_{a0}(R)}{X(R_m)}\exp\left\{2\int_{R_m}^R\left[S_{m0} - S_{a0}(x)\right]\beta_{m0}(x)dx\right\}. \qquad (4)$$

In the left-hand member of Eq. (4) we recognize that

$$S_{a0}(R)\left[\beta_{m0}(R)+\beta_{a0}(R)\right]\exp\left\{-2\int_{R_m}^{R}S_{a0}(x)\left[\beta_{a0}(x)+\beta_{m0}(x)\right]dx\right\}=$$
$$-\frac{1}{2}\frac{d}{dR}\exp\left\{-2\int_{R_m}^{R}S_{a0}(x)\left[\beta_{a0}(x)+\beta_{m0}(x)\right]dx\right\}, \tag{5}$$

with which Eq. (4) can be rewritten as

90

$$\frac{d}{dR}\exp\left\{-2\int_{R_m}^{R}S_{a0}(x)\left[\beta_{a0}(x)+\beta_{m0}(x)\right]dx\right\}=$$

$$-2\beta_{m0}(R_m)\frac{X(R)}{X(R_m)O(R)}S_{a0}(R)\exp\left\{2\int_{R_m}^{R}\left[S_{m0}-S_{a0}(x)\right]\beta_{m0}(x)dx\right\} \tag{6}$$

Integrating both members of Eq. (6) between R_m and R and rearranging terms one obtains

$$\exp\left\{-2\int_{R_m}^{R}S_{a0}(x)\left[\beta_{a0}(x)+\beta_{m0}(x)\right]dx\right\}=$$

$$1-2\frac{\beta_{m0}(R_m)}{X(R_m)}\int_{R_m}^{R}\frac{X(x)}{O(x)}S_{a0}(x)\exp\left\{2\int_{R_m}^{x}\left[S_{m0}-S_{a0}(x')\right]\beta_{m0}(x')dx'\right\}dx. \tag{7}$$

95 Substituting the right member of Eq. (7) for $\exp\left\{-2\int_{R_m}^{R}S_{a0}(x)\left[\beta_{a0}(x)+\beta_{m0}(x)\right]dx\right\}$ in the left-hand member of Eq. (4) and rearranging we arrive at

$$O(R)\left[\beta_{m0}(R)+\beta_{a0}(R)\right]=$$

$$\frac{\beta_{m0}(R_m)X(R)\exp\left\{2\int_{R_m}^{R}\left[S_{m0}-S_{a0}(x)\right]\beta_{m0}(x)dx\right\}}{X(R_m)-2\beta_{m0}(R_m)\int_{R_m}^{R}\frac{X(x)}{O(x)}S_{a0}(x)\exp\left\{2\int_{R_m}^{x}\left[S_{m0}-S_{a0}(x')\right]\beta_{m0}(x')dx'\right\}dx}. \tag{8}$$

Note that Eq. (8) is the Klett's solution of the lidar equation (Klett, 1985), (Sasano et al., 1985), except for the overlap
100 function appearing in its left-hand member and in the integral in the denominator in its right-hand member.

Now, from the Raman inversion method we obtain, assuming that the overlap functions of both the elastic and the Raman channels are the same, a backscatter coefficient not affected by the varying . overlap (Ansmann et al., 1992):

$$\beta_{a0}(R)+\beta_{m0}(R)=\frac{X(R)X_R(R_m)\beta_{m0}(R)}{X(R_m)X_R(R)}\frac{\exp\left\{-\int_{R}^{R_m}\left[\alpha_{a0}(x)+S_{m0}\beta_{m0}(x)\right]dx\right\}}{\exp\left\{-\int_{R}^{R_m}\left[\alpha_{aR}(x)+S_{mR}\beta_{mR}(x)\right]dx\right\}}, \tag{9}$$

with $X_R(R)$ the range-corrected Raman signal, $\alpha_{aR}(R)$ and $\beta_{mR}(R)$ the aerosol-extinction and the molecular-
105 backscatter coefficients respectively, both at the Raman-shifted wavelength λ_R, and S_{mR} the molecular lidar ratio at λ_R (D'Amico et al., 2016). If we divide Eq. (8) by Eq. (9), we arrive finally at the formula:

$$O(R)=\frac{\beta_{m0}(R_m)X(R_m)X_R(R)}{X_R(R_m)\beta_{m0}(R)}\times$$

$$\frac{\exp\left\{2\int_{R_m}^{R}[S_{a0}(x)-S_{m0}]\beta_{m0}(x)dx\right\}\exp\left\{\int_{R}^{R_m}[S_{m0}\beta_{m0}(x)-S_{mR}\beta_{mR}(x)]dx\right\}\exp\left\{\int_{R}^{R_m}[\alpha_{a0}(x)-\alpha_{aR}(x)]dx\right\}}{X(R_m)-2\beta_{m0}(R_m)\int_{R_m}^{R}\frac{X(x)}{O(x)}S_{a0}(x)\exp\left\{2\int_{R_m}^{x}[S_{a0}(x')-S_{m0}]\beta_{m0}(x')dx'\right\}dx}. \tag{10}$$

If we knew the aerosol differential transmission term $\exp\left\{\int_{R}^{R_m}[\alpha_{a0}(x)-\alpha_{aR}(x)]dx\right\}$ and the aerosol lidar ratio S_{a0} (the other terms are assumed to be known, because they are either measured or derived from radiosonde measurements), Eq. (10) could be solved iteratively for $O(R)$ by assuming an initial $O(R)$ in the right-hand member of Eq. (10) (e.g. $O(R)=1$, or the immediately previous overlap function assumed as valid for the system). This will give a new $O(R)$ estimate that would be substituted again in the right hand of Eq. (10), and the procedure will continue until $O(R)$ converges.

However, it is also possible to obtain an explicit expression for $O(R)$ by casting Eq. (10) into the form of a Volterra integral equation ((Mathews and Walker, 1970), section 11-5), which, in turn, can be converted into a first degree differential equation that can be integrated using standard techniques ((Mathews and Walker, 1970), section 1-1, see appendix A for details). To do that, we call

$$f(R)=\frac{1}{O(R)} \tag{11}$$

and define the functions $g(R)$, $\phi(R)$ and $\psi(R)$ as

$$g(R)=\frac{X_R(R_m)\beta_{m0}(R)}{\beta_{m0}(R_m)X_R(R)}\times$$

$$\exp\left\{-2\int_{R}^{R_m}[S_{a0}(x)-S_m(x)]\beta_{m0}(x)dx\right\}\exp\left\{-\int_{R}^{R_m}[S_{m0}\beta_{m0}(x)-S_{mR}\beta_{mR}(x)]dx\right\}\exp\left\{-\int_{R}^{R_m}[\alpha_{a0}(x)-\alpha_{aR}(x)]dx\right\}, \tag{12}$$

$$\phi(R)=\frac{2X_R(R_m)\beta_{m0}(R)}{X(R_m)X_R(R)}\times$$

$$\exp\left\{-2\int_{R}^{R_m}[S_{a0}(x)-S_m(x)]\beta_{m0}(x)dx\right\}\exp\left\{-\int_{R}^{R_m}[S_{m0}\beta_{m0}(x)-S_{mR}\beta_{mR}(x)]dx\right\}\exp\left\{-\int_{R}^{R_m}[\alpha_{a0}(x)-\alpha_{aR}(x)]dx\right\}, \tag{13}$$

and

$$\psi(R)=X(R)S_{a0}(R)\exp\left\{2\int_{R}^{R_m}[S_{a0}(x)-S_{m0}]\beta_{m0}(x)dx\right\}. \tag{14}$$

Then, following the steps detailed in appendix A, one arrives at the explicit form of the overlap function

$$O(R)=\frac{\beta_{m0}(R_m)X_R(R)}{\beta_m(R)X_R(R_m)}\times$$

$$\frac{\exp\left\{2\int_R^{R_m}\left[S_{a0}(x)-S_{m0}\right]\beta_{m0}(x)dx\right\}\exp\left\{\int_R^{R_m}\left[S_{m0}\beta_{m0}(x)-S_{mR}\beta_{mR}(x)\right]dx\right\}\exp\left\{\int_R^{R_m}\left[\alpha_{a0}(x)-\alpha_{aR}(x)\right]dx\right\}}{\exp\left\{2\frac{X_R(R_m)}{X(R_m)}\int_R^{R_m}\frac{S_{a0}(x)\beta_{m0}(x)X(x)}{X_R(x)}\exp\left(-\int_x^{R_m}\left[S_{m0}\beta_{m0}(x')-S_{mR}\beta_{mR}(x')\right]dx'\right)\exp\left(-\int_x^{R_m}\left[\alpha_{a0}(x')-\alpha_{aR}(x')\right]dx'\right)dx\right\}}$$

.

$$(15)$$

Note that every term in Eqs. (10) and (15), except the aerosol lidar ratio profile $S_{a0}(R)$ and the aerosol extinction coefficients, can be obtained either directly from the elastic and Raman lidar signals ($X(R)$ and $X_R(R)$), or calculated from the pressure and temperature provided by a radiosonde or by using a standard model of the atmosphere ($\beta_{m0}(R)$ and $\beta_{mR}(R)$). Note as well that, if a purely rotational Raman channel is used, the differential molecular and aerosol transmission terms, respectively $\exp\left\{\int_R^{R_m}\left[S_{m0}\beta_{m0}(x)-S_{mR}\beta_{mR}(x)\right]dx\right\}$ and $\exp\left\{\int_R^{R_m}\left[\alpha_{a0}(x)-\alpha_{aR}(x)\right]dx\right\}$, can be safely ignored in Eqs. (10) and (15). In appendix B we assess the error committed when a vibro-rotational Raman channel is used and the wavelength differences cannot be longer neglected.

Although based on the same principles as the iterative method proposed in (Wandinger and Ansmann, 2002), the formulation of Eq. (15) has the advantages of not requiring iterations (admittedly, not a decisive issue with the current computing technology) and, more important, of providing insight on the effect of the assumed aerosol lidar ratio on the retrieved overlap function (see section 3) and on the systematic error incurred when the differential aerosol transmission at the emitted and Raman wavelengths cannot be neglected (see appendix B).

3. Influence of the lidar ratio

To assess the influence of the assumed lidar ratio on the overlap function retrieval we substitute in Eq. (10) the expressions of $X(R)$ and $X_R(R)$ that would correspond to a given aerosol distribution,

$$X(R) = A\,O(R)\left[\beta_{m0}(R)+\beta_{a0}(R)\right]\exp\left\{-2\int_0^R\left[\alpha_{a0}(x)+S_{m0}\beta_{m0}(x)\right]dx\right\}, \tag{16a}$$

$$X_R(R) = B\,O(R)\beta_{mR}(R)\exp\left\{-\int_0^R\left[\alpha_{a0}(x)+\alpha_{aR}(x)\right]+\left[S_{m0}\beta_{m0}(x)+S_{mR}\beta_{mR}(x)\right]dx\right\}, \tag{16b}$$

where A and B are instrument constants. We also assume that we may use an "erroneous" lidar ratio

$$S'_{a0}(R) = S_{a0}(R)+\Delta S_{a0}(R), \tag{17}$$

where $S_{a0}(R)$ is the "true" lidar ratio (actually unknown) and $\Delta S_{a0}(R)$ the deviation from it. Using $S'_{a0}(R)$ in Eq. (15), and replacing in it the expressions of $X(R)$ and $X_R(R)$ given by Eqs. 16. we find, after some boring and cumbersome, but otherwise straightforward, algebraic developments, the surprisingly simple result

$$O'(R) = O(R)\exp\left[-2\int_R^{R_m}\Delta S_{ao}(x)\beta_{ao}(x)dx\right], \tag{18}$$

where $O'(R)$ is the overlap function found, different from the true one, $O(R)$, because of the error ΔS_{a0} in the lidar ratio.

One reaches the following conclusions from Eq. (18):

a) If the atmosphere measured to retrieve the overlap function were aerosol-free, i.e. $\beta_{a0}(R)=0$ for all ranges, the assumed lidar ratio (hence ΔS_{a0}) would be irrelevant, since Eq. (18) would lead to $O'(R)=O(R)$.

b) Likewise, if there is no aerosol for any range $R_T < R < R_m$, in that range $O'(R) = O(R)$ regardless of the assumed lidar ratio.

c) If $\Delta S_{a0}(x) > 0$, then $O'(R) < O(R)$ in the range with aerosol.

d) If $\Delta S_{a0}(x) < 0$, then $O'(R) > O(R)$ in the range with aerosol.

Note that, because β_{a0} tends to be larger at shorter wavelengths, the sensitivity of the retrieved overlap function to an error in the assumed lidar ratio is expected to be larger at shorter wavelengths.

4.   Example results

We have used Eq. (15) to obtain estimates of the overlap function at 355 nm and 532 nm of the lidar of the Universitat Politècnica de Catalunya (UPC), an eight-channel multispectral combined Raman-elastic backscatter lidar that is described in (Kumar et al., 2011), with the modification in the UV branch of the wavelength separation unit described in ref. (Zenteno-Hernández et al., 2021) to implement a N_2/O_2 purely rotational Raman channel at 354 nm. This instrument belongs to the EARLINET European aerosol lidar network, currently integrated into the Aerosol, Clouds and Trace Gases Research Infrastructure (ACTRIS). To retrieve the overlap function at 355 nm, we have used the purely rotational Raman channel, which provides a higher signal-to-noise ratio than the vibro-rotational one (Zenteno-Hernández et al., 2021). For the overlap function at 532 nm we used the elastic signal return and the signal of the N_2 vibro-rotational Raman channel at 607 nm.

To illustrate the effect of the assumed aerosol lidar ratio, we have chosen two nighttime measurements (60-minute measurement on 11th November 2021 starting at 20:41 UTC and 60-minute measurement on 1st December 2021 starting at 1:44) corresponding to situations with relatively low aerosol load.

Figure 1 presents the range-corrected, Rayleigh-fitted lidar signals used for computing the overlap profiles. The 11 November signals were fitted to the Rayleigh profile between 4 and 6 km, because of the presence of clouds (partially visible in the plot) from 6.3 km upwards. The 1 December signals were fitted between 7 and 11 km. In both cases, the lidar signals fit to the Rayleigh profile with great accuracy in the interval from 4 to 6 km (to 8 km in the case of 1 December), indicating an aerosol-free atmosphere.

Figure 2 presents the backscatter coefficients obtained with the Raman method (Eq. (9), no smoothing applied to the signals) at 355 nm and 532 nm neglecting the difference between the aerosol extinction coefficients at the emitted and Raman wavelengths. Note that this approximation is very well justified when the Raman channel is a purely rotational one, as in the case of the backscatter coefficient at 355 nm, since the two signals employed are at almost the same wavelength. Figure. 2 shows that the aerosol backscatter coefficient at both wavelengths was much lower for the 1st of December measurement than for the 11th of November one. It also shows that the backscatter coefficient for the same day is higher at the shorter wavelength. Fig. 2 warns also on a possible breakdown of the equal overlap function hypothesis for the elastic and Raman channels, more clearly seen examining the profiles of 1st of December: while the 532-nm aerosol backscatter coefficient shows a reasonable behavior until very low altitudes, the 355-nm one has a sudden fall below approximately 400 m. For this reason, in this particular case of optical alignment we should distrust the overlap function retrieval below that height for all cases.

Figure 3 shows the results of the overlap function retrieval with our formulation (Eq. (15)), neglecting the differential aerosol transmissions (terms $\exp\left\{\int_R^{R_m}[\alpha_{a0}(x) - \alpha_{aR}(x)]dx\right\}$ assumed 1; see appendix B for the assessment of the error bound entailed by this assumption) for three "reasonable" lidar ratios (25 sr, 50 sr and 75 sr) from the 11th of November 2021 measurement. The reference height is taken at 6 km, where the Rayleigh fit of the signals indicate absence of aerosol (in agreement with the profiles of figs. 1 & 2). The detected lidar signal sequences are noisy, especially the Raman ones, whereas the overlap function cannot have steep or sudden variations at far ranges; therefore, a smoothing procedure, coupled with a Monte Carlo routine to assess the residual error bars, has been employed. An overlap profile retrieved with the original noisy sequences (only for 50 sr lidar ratio) is plotted as well.
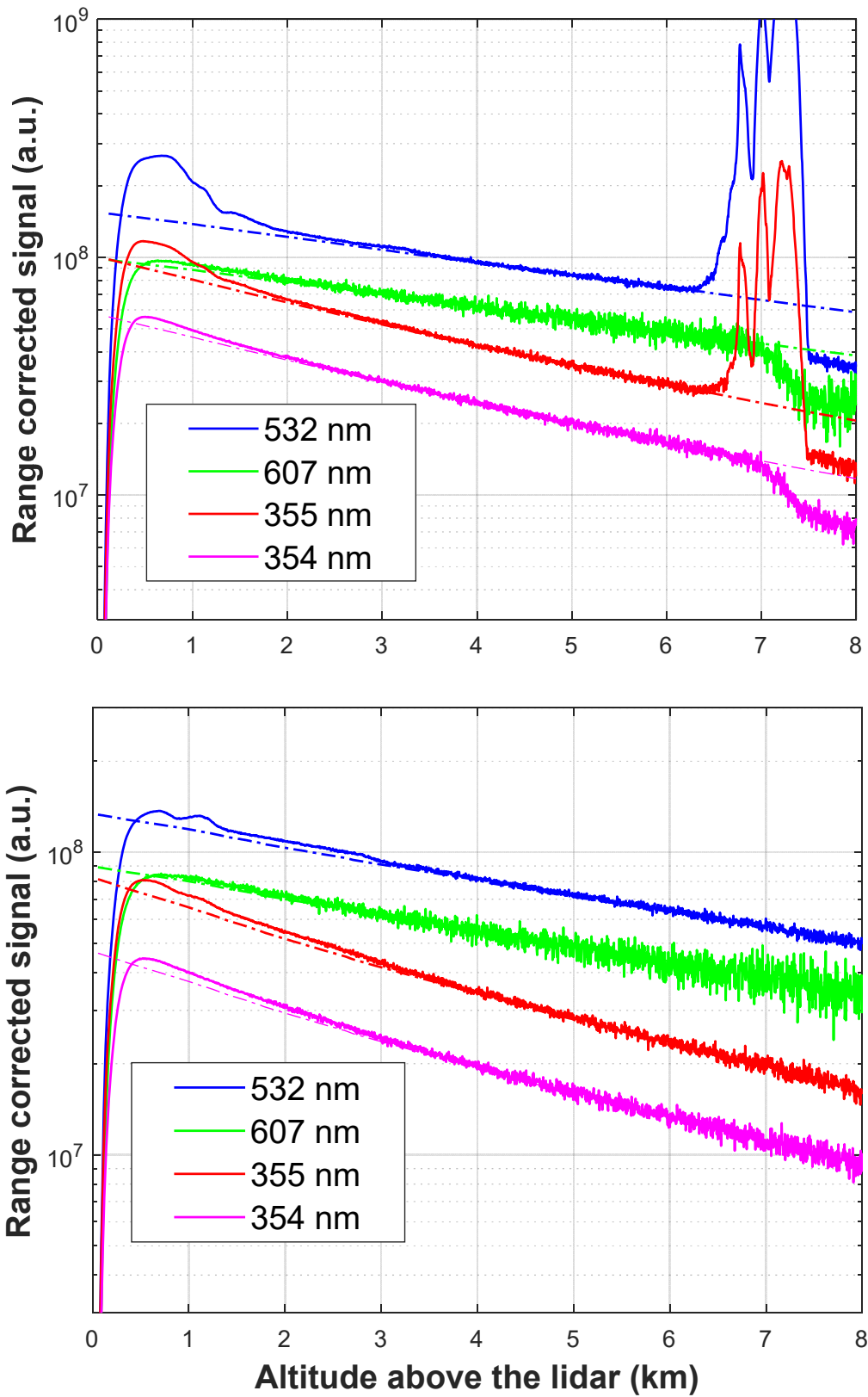
Fig. 1. Range-corrected, Rayleigh-fitted lidar signals used in the example. The lidar signals (plotted with solid line) were fitted to a Rayleigh profile (plotted with dash-dot line) obtained from the closest available radiosonde. Upper graph: signals from 11 November 2021 measurement at 20:41 UTC, with radiosonde from 12 November 2021 at 00:00 UTC. Lower graph: signals from 1 December 2021 measurement at 01:44 UTC, with radiosonde from 1 December 2021 at 00:00 UTC.

The raw elastic and Raman signal sequences detected by our lidar were fitted to a Rayleigh reference profile obtained from a nearby radio-sound. The sequences were corrected in range as well, being all these processes common in lidar inversion techniques. The result of this process leads to $X(n)$ and $X_R(n)$, standing for elastic and Raman signal sequences. Previous ("noisy") estimates of the overlap profiles were calculated with these sequences.

These sequences were then smoothed to reduce the remaining noise, especially in the segments corresponding to high altitudes. This smoothing uses an adaptive sliding average approach. Each sample of the smoothed sequence was calculated as

$$X_{X\_sm}(n) = \frac{1}{L+1} \sum_{i=n-L/2}^{n+L/2} X_X(i), \tag{19}$$

where the sub-index X stands for either elastic or Raman. The averaging window length L varies from 1 to 150 (3.75 m to 562.5 m considering the raw range resolution of our lidar) as n grows. For low altitudes (low n) the noise is not significant and the expected lidar signals show relevant variations, so L must be short, while it can be made longer for sequence segments corresponding to farther ranges, especially in the molecular zone.

The noise of these signals is estimated by comparing the non-smoothed sequences with the smoothed one. The estimation of this noise is necessary to create the different realizations in a Monte Carlo strategy to compute the error bars of the overlap estimation. Considering that the sequences have been smoothed by performing a $(L+1)$-long average, the standard deviation of the n-th sample is estimated as (Papoulis and Pillai, 2002):

$$\Delta X_X(n) = \frac{1}{\sqrt{L+1}} \sqrt{\frac{1}{2L+1} \sum_{i=n-L}^{n+L} \left[X_X(i) - X_{X\_sm}(i) \right]^2} \; . \tag{20}$$

The uncertainty of the calculated overlap profiles is estimated by using a common Monte Carlo approach. With the statistics obtained with equations (19) and (20), N_{MC} (usually $N_{MC} \approx 100$) pairs of elastic and Raman signal statistically independent sequences are synthesized. Each of these synthesized sequences are generated as

$$X_{X\_k}(n) = X_{X\_sm}(n) + e_{X\_k}(n), \tag{21}$$

where each $e_{X\_k}(n)$ is a realization of a Gaussian random variable with zero average and standard deviation $\Delta X_X(n)$.

With these N_{MC} sequence pairs, N_{MC} overlap profiles $Ov_k(n)$ are calculated. The average overlap profiles $Ov(n)$ and error bars $\Delta Ov(n)$ presented in the next figures have been calculated as (Papoulis and Pillai, 2002):

$$Ov(n) = \frac{1}{N_{MC}} \sum_{k=1}^{100} Ov_k(n) \tag{22}$$

$$\Delta Ov(n) = \sqrt{\frac{\sum_{k=1}^{N_{MC}} \left[Ov_k(n) - Ov(n) \right]^2}{(N_{MC}-1)}} \tag{23}$$

235
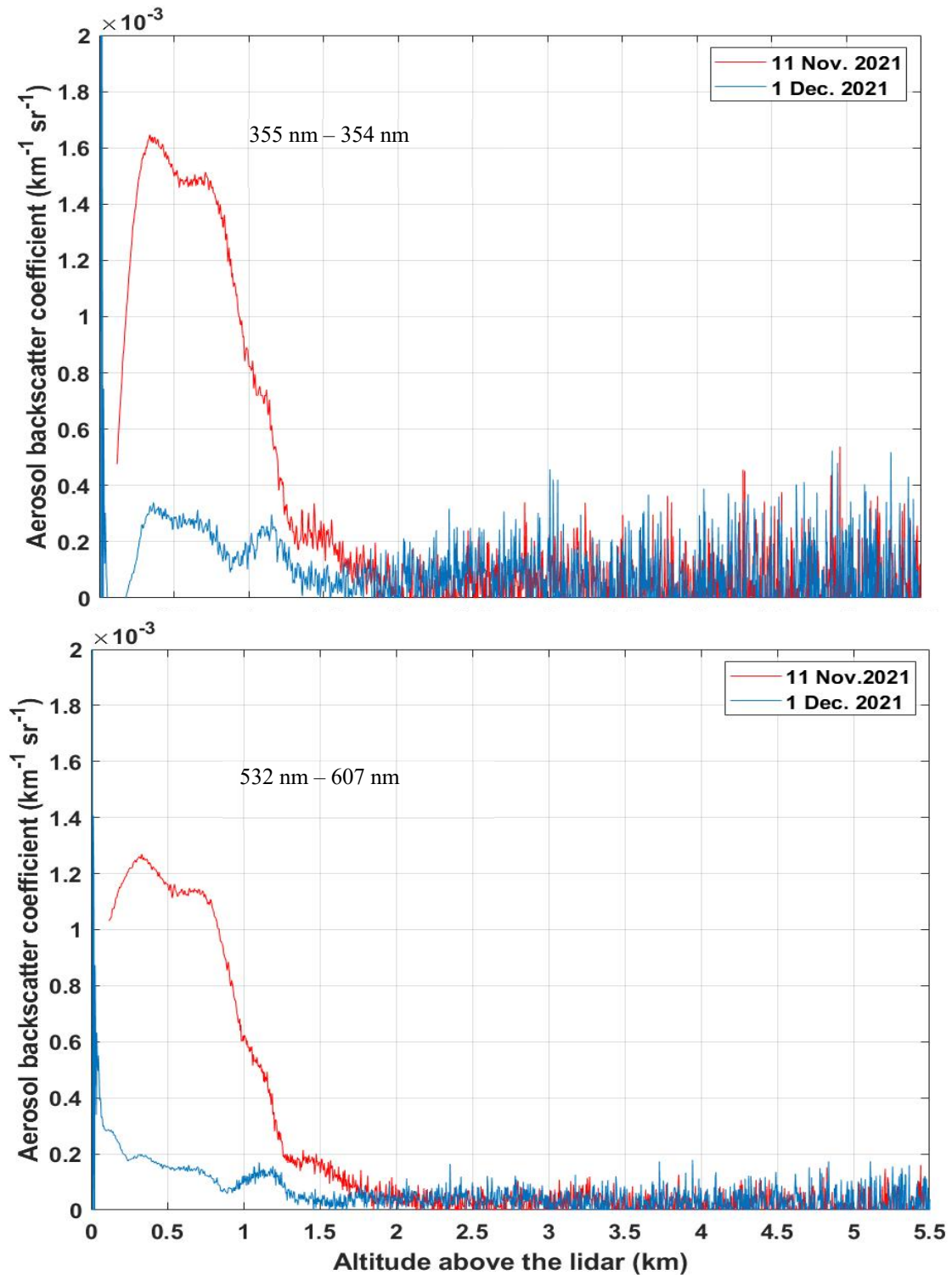
Fig. 2. Aerosol backscatter coefficient using the Raman method formula. Upper graph: nominally at 355 nm using the 355 nm elastic channel and the 354 purely rotational channel. Lower graph: nominally at 532 nm using the 532 nm elastic channel and the 607 nm vibro-rotational Raman channel.
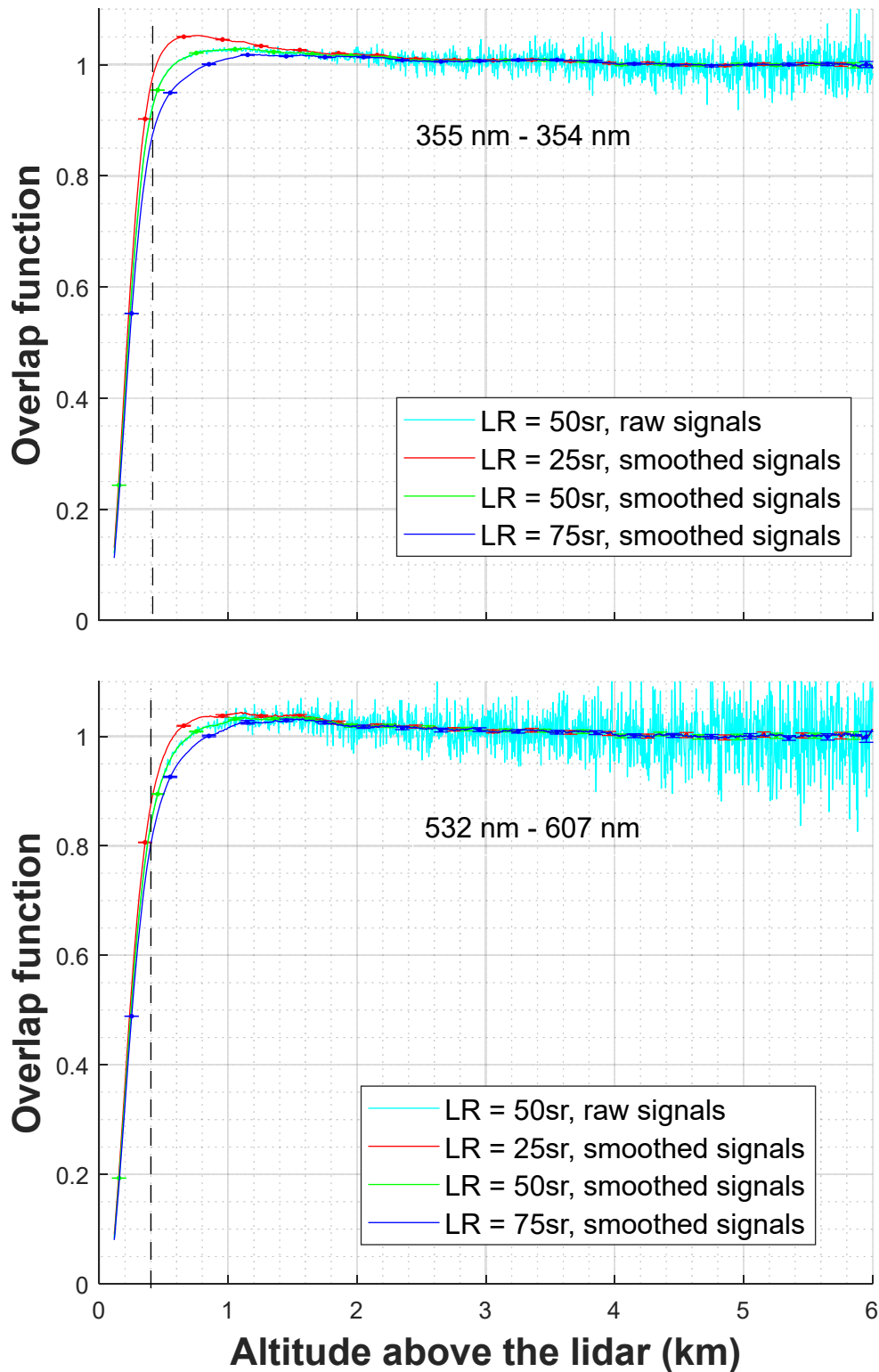
Fig. 3. Overlap functions retrieved assuming different lidar ratios (LR) at 355 nm (upper panel) and 532 nm (lower panel) from measurements carried out on 11th of November 2021. A smoothing procedure described in the text has been applied and error bars are shown. As a reminder of the applied smoothing a raw result for a 50-sr lidar ratio is shown in grey. The vertical discontinuous line marks the 400-m height below which the correction is to be mistrusted.
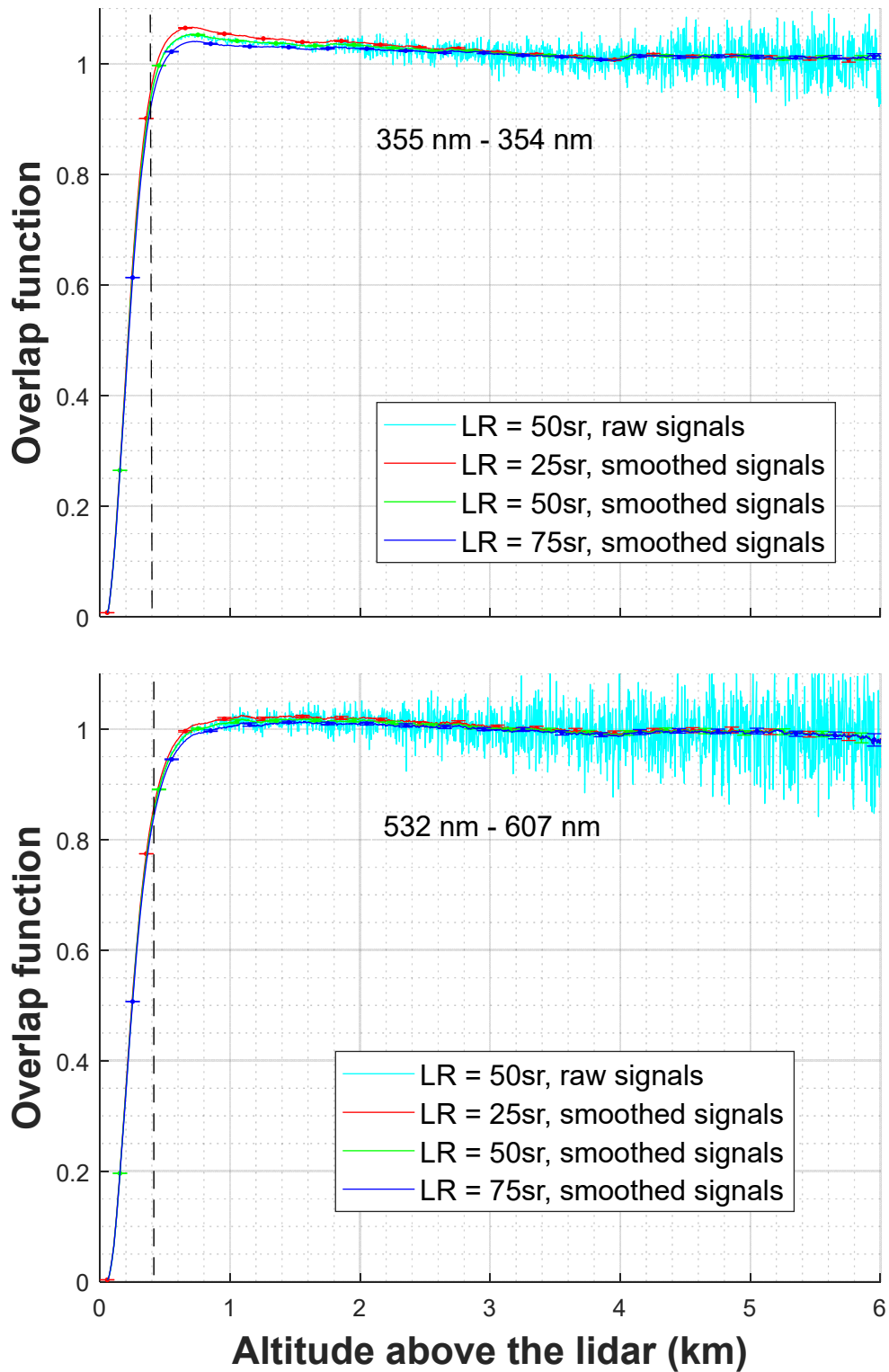
Fig. 4. Overlap functions retrieved assuming different lidar ratios (LR) at 355 nm (upper panel) and 532 nm (lower panel) from measurements carried out on 1st of December 2021. The same smoothing procedure and method to obtain error bars as in fig. 2 have been employed. As in fig. 2, the vertical dashed line marks the range below which the retrieval is subject to caution. As a reminder of the applied smoothing a raw result for a 50-sr lidar ratio is shown in grey.

In fig. 4 the retrieved overlap functions from data of the 1ˢᵗ of December 2021 are represented for the same assumed lidar ratios as in figure 3. Because we have arbitrarily normalized the profile to the reference height, where the overlap function has reached a stable value, values greater than one, as shown in figs. 2 and 3, at lower ranges are possible and reveal a non-perfect alignment, in particular, a slight crossing between the laser beam and the receiver field-of-view axes, leading to a loss of energy from the far range (see for example fig 1(a) in (Kokkalis, 2017) with laser tilt A_{tilt}, half-width laser beam divergence LBD and receiver field of view $RFOV$ fulfilling the conditions $A_{tilt} + LBD > RFOV$ and $A_{tilt} - LBD < RFOV$). As expected (section 3), being the aerosol backscatter coefficients at both wavelengths lower in this measurement, the difference between the overlaps obtained with different lidar ratios is lower than for the 11ᵗʰ of November. Also, because the backscatter coefficient at 532 nm is lower than at 355 nm, the differences of the retrieved overlap functions are less sensitive to the guessed lidar ratio at the former wavelength, being in fact almost negligible. An overlap profile retrieved with the original noisy sequences (for LR = 50 sr) is plotted as well. Although using a different, explicit, non-iterative formulation, the method presented in this paper relies on the same basis as the one given by Wandinger and Ansmann. The reader can check that, for the same measured data and assumed lidar ratio, both methods, for a sufficient number of iterations in (Wandinger and Ansmann, 2002), yield indistinguishable results.

5. Conclusions

Based on same principle as in ref. (Wandinger and Ansmann, 2002). i.e. that the aerosol backscatter coefficient derived by the Raman method (Ansmann et al., 1992) is not affected by the lidar range-varying overlap (under the assumption of the same overlap function for the elastic and the Raman channels), a new formulation for deriving the overlap function of an aerosol lidar system equipped with Raman channels has been presented. As input data, the method uses the elastic and the Raman signals and a guess of the lidar ratio corresponding to the emitted wavelength of interest. The novelty of our approach consists in the derivation of an explicit formula in which no iterations have to be performed.

Results of the formula are illustrated with two examples, both with low aerosol load, but one of them with a much lower load than the other, showing the effect of the guessed lidar ratio on the overlap function retrievals.

The explicit formula allows one to assess the errors committed when an erroneous lidar ratio is used (section 3), showing, as already stated by (Wandinger and Ansmann, 2002), that the retrieval of the overlap function is less prone to errors when performed in clear atmospheres. It also makes it possible to find systematic error bounds associated to the uncertainty in the different aerosol transmissions at the elastic and the Raman wavelengths when Raman vibro-rotational channels are used (appendix B).Section 3 also cautions against trying to derive a lidar ratio using the corrected-for-overlap signal. Actually, one could be tempted to think of the following procedure: an overlap function is retrieved using a guessed aerosol lidar ratio; with that overlap function, the Raman signal is corrected and an aerosol extinction coefficient is calculated, which, divided by the aerosol backscatter, gives a new lidar ratio, which is turn used to retrieve a new overlap function, and so on. However, Eq. (18) shows that this procedure does not converge, for, if a too low lidar ratio is used as first guess, the overlap function will be enhanced in the range with aerosol; when correcting with this enhanced overlap function, the Raman signal will be suppressed, which will give rise to an aerosol extinction coefficient lower than due and, consequently to a lower new lidar ratio. A similar reasoning goes on if the guessed aerosol lidar ration is too high. The determination of the required lidar ratio from Raman inversions needs atmospheric regions with both significant aerosol load and stable overlap. However, in cases with regions where both conditions are fulfilled, using the retrieved lidar ratio for overlap estimations requires assuming that the type of aerosol is uniform down to the ground. Moreover, as seen in section 3, in aerosol loaded scenarios, errors in the lidar ratio determination yield greater errors in the estimation of the overlap profile. A more conservative approach is to stay with situations with low aerosol load at low altitudes and use the aerosol backscatter profiles derived with the Raman method (e.g. fig. 2). together with a sun- or lunar-photometer AOD measurement, and find the aerosol lidar ratio that, multiplied by the integrated aerosol backscatter coefficient would, would yield the AOD measured by the photometer. However, these techniques are out of the scope of this paper, which aims only at presenting the explicit formulation of the overlap function and discussing the effect of the assumed lidar ratio on the retrieved profiles.

6.   Appendix A: derivation of the explicit form of the overlap function

We outline here the mathematical details to obtain Eq. (15). Using the definitions of Eqs. (12), (13) and (14), Eq. (10) can be written as the Volterra integral equation

$$f(R) = g(R) + \phi(R) \int_R^{R_m} f(x)\psi(x)\,dx,$$ (A1)

which is amenable to a differential equation. In order to do that, we define the function

$$u(R) = \int_R^{R_m} f(x)\psi(x)\,dx,$$ (A2)

which, substituting into Eq. (A1), yields

$$f(R) = g(R) + u(R)\phi(R).$$ (A3)

We next take the derivative Eq. (A2):

$$\frac{d}{dR}u(R) = -f(R)\psi(R)$$ (A4)

and substitute Eq. (A3) on it to obtain, after reordering terms

$$\frac{d}{dR}u(R) + \phi(R)\psi(R)u(R) = -g(R)\psi(R).$$ (A5)

To integrate that equation, we define an integrating factor $\exp\left[\int_R^{R_m}\phi(x)\psi(x)\,dx\right]$ and multiply both members of Eq. (A5) by it, which allows us to recast the equation as

$$\frac{d}{dR}\left\{u(R)\exp\left[\int_R^{R_m}\phi(x)\psi(x)\,dx\right]\right\} = -g(R)\psi(R)\exp\left[\int_R^{R_m}\phi(x)\psi(x)\,dx\right].$$ (A6)

Integrating both members of Eq. (A6) between R and R_m, and noting that, by construction, $u(R_m) = 0$, leads to

$$u(R) = \exp\left[\int_R^{R_m}\phi(x)\psi(x)\,dx\right]\int_R^{R_m} g(x)\psi(x)\exp\left[-\int_x^{R_m}\phi(x')\psi(x')\,dx'\right]dx.$$ (A7)

Finally, taking the derivatives of both members of Eq. (A7) and considering Eq. (A4) one obtains

$$f(R) = g(R) + \phi(R)\exp\left[\int_R^{R_m}\phi(x)\psi(x)\,dx\right]\int_R^{R_m} g(x)\psi(x)\exp\left[-\int_x^{R_m}\phi(x')\psi(x')\,dx'\right]dx.$$ (A8)

In our case, $g(R) = \frac{1}{2}\frac{X(R_m)}{\beta_{m0}(R_m)}\phi(R)$ (see Eqs. (12) and (13)), which makes

$$O(R) = \frac{1}{f(R)} = \frac{2\beta_{m0}(R_m)}{X(R_m)\phi(R)\exp\left[\int_R^{R_m}\phi(x)\psi(x)\,dx\right]}.$$ (A9)

7.   Appendix B: Systematic error bounds

We assess the error incurred in the estimation of $O(R)$ (Eq. (15)) when neglecting the difference in molecular lidar ratios and the differential aerosol transmission term.

We start by noting that (Bucholtz, 1995; D'Amico et al., 2016) the molecular lidar ratio at a wavelength λ can be written as

$$S_{m\lambda} = S_m \left(1 + \frac{\delta_{n\lambda}}{2}\right), \tag{B1}$$

with $S_m = \frac{8\pi}{3}$ and $\delta_{n\lambda}$ is the depolarization factor that takes into account the anisotropy of the air molecules (Bucholtz, 1995). We can then write the terms $S_{m0}\beta_{m0}(x) - S_{mR}\beta_{mR}(x)$ in Eq. (15) as

$$S_{m0}\beta_{m0}(x) - S_{mR}\beta_{mR}(x) = S_m\left[\beta_{m0}(x) - \beta_{mR}(x)\right] + \frac{S_m}{2}\left[\delta_{n0}\beta_{m0}(x) - \delta_{nR}\beta_{mR}(x)\right], \tag{B2}$$

315 where, for a vibro-rotational Raman channel, $\frac{S_m}{2}\left[\delta_{n0}\beta_{m0}(x) - \delta_{nR}\beta_{mR}(x)\right] > 0$.

The terms $\alpha_{a0}(x) - \alpha_{aR}(x)$ can be written

$$\alpha_{a0}(x) - \alpha_{aR}(x) = \left[1 - \left(\frac{\lambda_0}{\lambda_R}\right)^{a(x)}\right]\alpha_{a0}(x), \tag{B3}$$

with $a(x)$ the Ångström exponent, which is in general positive.

By examining Eq. (15) and Eqs. (B2) and (B3) it is seen that

320 $$O(R) > O_0(R), \tag{B4}$$

with $O_0(R)$ defined as

$$O_0(R) = \frac{\beta_{m0}(R_m)X_R(R)}{\beta_m(R)X_R(R_m)} \frac{\exp\left\{2\int_R^{R_m}\left[S_{a0}(x) - S_{m0}\right]\beta_{m0}(x)dx\right\}\exp\left\{S_m\int_R^{R_m}\left[\beta_{m0}(x) - \beta_{mR}(x)\right]dx\right\}}{\exp\left\{2\frac{X_R(R_m)}{X_m}\int_R^{R_m}\frac{S_{a0}(x)\beta_{m0}(x)X(x)}{X_R(x)}\exp\left(-S_m\int_x^{R_m}\left[\beta_{m0}(x') - \beta_{mR}(x')\right]dx'\right)dx\right\}}, \tag{B5}$$

i.e. ignoring the difference in the aerosol transmissions at the elastic and Raman wavelengths, and

$$O(R) < O_0(R) \times$$

325 $$\frac{\exp\left\{\frac{S_m}{2}\int_R^{R_m}\left[\delta_{n0}\beta_{m0}(x) - \delta_{nR}\beta_{mR}(x)\right]dx\right\}\exp\left\{\left[1 - \left(\frac{\lambda_0}{\lambda_R}\right)^{a_{max}}\right]AOD_0\right\}}{\exp\left\{2\frac{X_R(R_m)}{X_m}\int_R^{R_m}\frac{S_{a0}(x)\beta_{m0}(x)X(x)}{X_R(x)}\exp\left(-S_m\int_x^{R_m}\left[\beta_{m0}(x') - \beta_{mR}(x')\right]dx'\right)dx\right\}^{\exp\left\{-\frac{S_m}{2}\int_R^{R_m}\left[\delta_{n0}\beta_{m0}(x) - \delta_{nR}\beta_{mR}(x)\right]dx\right\}\exp\left\{-\left[1 - \left(\frac{\lambda_0}{\lambda_R}\right)^{a_{mx}}\right]AOD_0\right\}-1}}, \tag{B6}$$

with AOD_0 the aerosol optical depth at the wavelength λ_0 and a_{max} the maximum Ångström exponent found along the lidar line of sight.

As an example, the upper bound factor $O(R)/O_0(R)$ according to Eq. (B6), with the data used to obtain the lower panel of fig. 3 and $S_a = 50$ sr, $AOD_0 = 0.05$ and $a_{max} = 1.3$ is given in fig. B1. We see as well that considering $S_{m0} = S_{mR} = S_m$

330 has only a small impact in the bound.
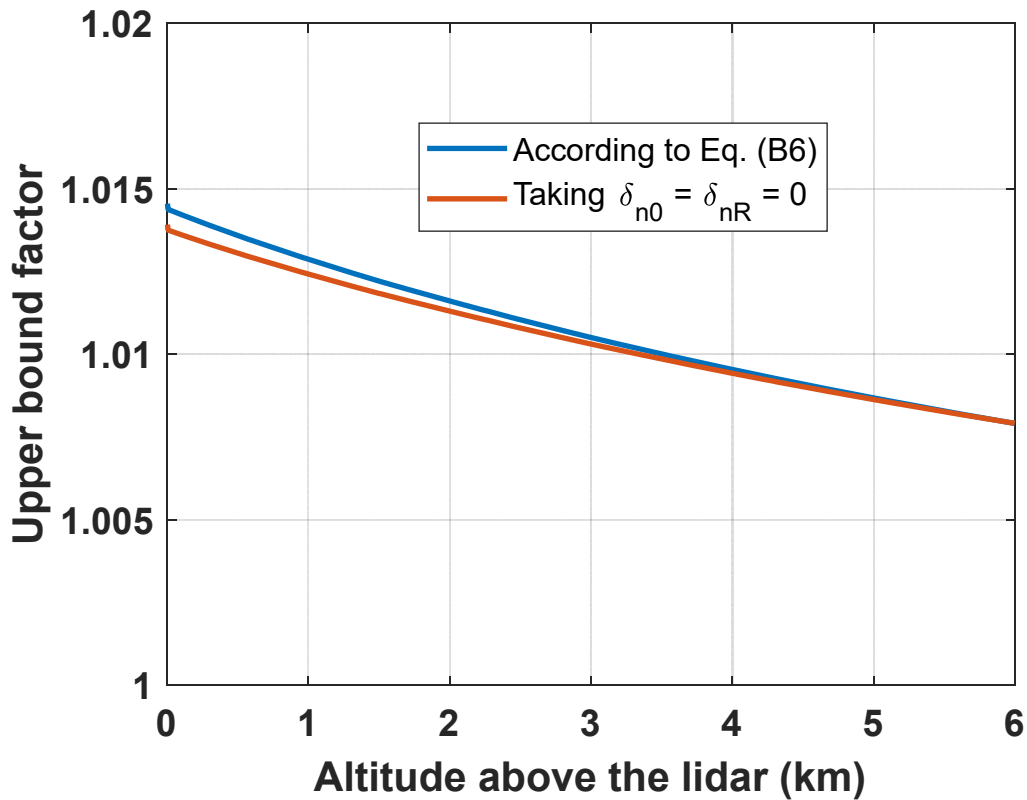
Fig. B1. Upper bound factor of the overlap function obtained with the wavelength combination 532 nm – 607 nm for the measurement of 1 December 2021, assuming a 50-sr aerosol lidar ratio, a 0.05 aerosol optical depth and a 1.3 maximum Ångström exponent.

8. Data availability

The range-corrected signals used for the overlap function retrievals can be downloaded from https://doi.org/10.34810/data704

335

9. Author contributions

Adolfo Comerón developed the new formulation, the software needed and the overall concept, he wrote part of the text and generated figures 2 and B1. Constantino Muñoz contributed with data analysis and wrote some parts of the text. Alejandro Rodríguez developed the Monte Carlo approach to smooth the overlap profiles and calculating the error bars; he generated figures 1, 3 and 4. The contributions of Michaël Sicard, Federico Dios, Cristina Gil-Díaz, Daniel Camilo Fortunato Dos Santos Oliveira and Francesc Rocadenbosch have been invaluable in the inception, development and consolidation of our lidar system, besides the contribution in measurements, data analysis and selection of the most appropriate cases for the retrieval of the overlap profiles.

340

345 ## 10. Competing interests

The authors declare that they do not have any competing interests.

11. Acknowledgements

350 The authors acknowledge the funding of this research by the Spanish State Agency for Research (AEI) for the project PID2019-103886RB-I00 and the support of the Ministry for Science and Innovation to ACTRIS ERIC. The authors also acknowledge the support of the European Commission through the Horizon 2020 Research and Innovation Framework Programme projects ACTRIS IMP (grant agreement No 871115), ATMO-ACCESS (grant agreement No 101008004) and GRASP-ACE (grant agreement No 778349).

355

12. References

360 Ancellet, G. M., Kavaya, M. J., Menzies, R. T., and Brothers, A. M.: Lidar telescope overlap function and effects of misalignment for unstable resonator transmitter and coherent receiver, Appl. Opt., 25, 2886–2890, https://doi.org/10.1364/AO.25.002886, 1986.

Ansmann, A., Wandinger, U., Riebesell, M., Weitkamp, C., and Michaelis, W.: Independent measurement of extinction and backscatter profiles in cirrus clouds by using a combined Raman elastic-backscatter lidar., Appl. Opt., 31, 7113, https://doi.org/10.1364/AO.31.007113, 1992.

365 Bucholtz, A.: Rayleigh-scattering calculations for the terrestrial atmosphere, Appl. Opt., 34, 2765, https://doi.org/10.1364/ao.34.002765, 1995.

Comeron, A., Sicard, M., Kumar, D., and Rocadenbosch, F.: Use of a field lens for improving the overlap function of a lidar system employing an optical fiber in the receiver assembly, Appl. Opt., 50, 5538–5544, https://doi.org/10.1364/AO.50.005538, 2011.

370 D'Amico, G., Amodeo, A., Mattis, I., Freudenthaler, V., and Pappalardo, G.: EARLINET Single Calculus Chain-technical andndash; Part 1: Pre-processing of raw lidar data, Atmos. Meas. Tech., 9, 491–507, https://doi.org/10.5194/amt-9-491-2016, 2016.

Dho, S. W., Park, Y. J., and Kong, H. J.: Experimental determination of a geometric form factor in a lidar equation for an inhomogeneous atmosphere, Appl. Opt., 36, 6009, https://doi.org/10.1364/AO.36.006009, 1997.

375 Engelmann, R., Kanitz, T., Baars, H., Heese, B., Althausen, D., Skupin, A., Wandinger, U., Komppula, M., Stachlewska, I. S., Amiridis, V., Marinou, E., Mattis, I., Linné, H., and Ansmann, A.: The automated multiwavelength Raman polarization and water-vapor lidar PollyXT: The neXT generation, Atmos. Meas. Tech., 9, 1767–1784, https://doi.org/10.5194/amt-9-1767-2016, 2016.

Gimmestad, G. G. and Roberts, D. W.: Teaching lidar inversions, in: Proceedings of the 25th International Laser Radar 380 Conference, 190–191, 2010.

Guerrero-Rascado, J. L., Costa, M. J., Bortoli, D., Silva, A. M., Lyamani, H., and Alados-Arboledas, L.: Infrared lidar overlap function: an experimental determination, Opt. Express, 18, 20350–20369, https://doi.org/10.1364/OE.18.020350, 2010.

Halldórsson, T. and Langerholc, J.: Geometrical form factors for the lidar function, Appl. Opt., 17, 240, 385 https://doi.org/10.1364/ao.17.000240, 1978.

Vande Hey, J., Coupland, J., Foo, M. H., Richards, J., and Sandford, A.: Determination of overlap in lidar systems, Appl. Opt., 50, 5791–5797, https://doi.org/10.1364/AO.50.005791, 2011.

Hu, S., Wang, X., Wu, Y., Li, C., and Hu, H.: Geometrical form factor determination with Raman backscattering signals, Opt. Lett., 30, 1879–1881, https://doi.org/10.1364/OL.30.001879, 2005.

390 Klett, J. D.: Lidar inversion with variable backscatter/extinction ratios, Appl. Opt. Vol. 24, Issue 11, pp. 1638-1643, 24, 1638–1643, https://doi.org/10.1364/AO.24.001638, 1985.

Kokkalis, P.: Using paraxial approximation to describe the optical setup of a typical EARLINET lidar system, Atmos.

Meas. Tech., 10, 3103–3115, https://doi.org/10.5194/amt-10-3103-2017, 2017.

Kumar, D. and Rocadenbosch, F.: Determination of the overlap factor and its enhancement for medium-size tropospheric lidar systems: a ray-tracing approach, J. Appl. Remote Sens., 7, 1–15, https://doi.org/10.1364/AO.50.005538, 2013.

Kumar, D., Rocadenbosch, F., Sicard, M., Comeron, A., Muñoz, C., Lange, D., Tomás, S., and Gregorio, E.: Six-channel polychromator design and implementation for the UPC elastic/Raman lidar, 81820W, https://doi.org/10.1117/12.896305, 2011.

Kuze, H., Kinjo, H., Sakurada, Y., and Takeuchi, N.: Field-of-view dependence of lidar signals by use of Newtonian and Cassegrainian telescopes, Appl. Opt., 37, 3128–3132, https://doi.org/10.1364/AO.37.003128, 1998.

Lefrère, J.: Etude par sondage laser de la basse atmosphère, Univeriste de Paris 6, 1982.

Li, J., Li, C., Zhao, Y., Li, J., and Chu, Y.: Geometrical constraint experimental determination of Raman lidar overlap profile, Appl. Opt., 55, 4924, https://doi.org/10.1364/ao.55.004924, 2016.

Mahagammulla Gamage, S., Sica, R. J., Martucci, G., and Haefele, A.: Retrieval of temperature from a multiple channel pure rotational Raman backscatter lidar using an optimal estimation method, Atmos. Meas. Tech., 12, 5801–5816, https://doi.org/10.5194/amt-12-5801-2019, 2019.

Mathews, J. and Walker, R. L.: Mathematical Methods of Physics, 2nd ed., The Benjamin/Cummings Publishing Company, 1970.

Di Paolantonio, M., Dionisi, D., and Liberti, G. L.: A semi-automated procedure for the emitter-receiver geometry characterization of motor-controlled lidars, Atmos. Meas. Tech., 15, 1217–1231, https://doi.org/10.5194/amt-15-1217-2022, 2022.

Papoulis, A. and Pillai, S. U.: Probability, random variables, and stochastic processes, 4th ed., McGraw-Hill, 2002.

Povey, A. C., Grainger, R. G., Peters, D. M., Agnew, J. L., and Rees, D.: Estimation of a lidar's overlap function and its calibration by nonlinear regression, Appl. Opt., 51, 5130–5143, https://doi.org/10.1364/AO.51.005130, 2012.

Sasano, Y., Shimizu, H., Takeuchi, N., and Okuda, M.: Geometrical form factor in the laser radar equation: an experimental determination, Appl. Opt., 18, 3908, https://doi.org/10.1364/ao.18.003908, 1979.

Sasano, Y., Browell, E. V., and Ismail, S.: Error caused by using a constant extinction/backscattering ratio in the lidar solution, Appl. Opt., 24, 3929, https://doi.org/10.1364/ao.24.003929, 1985.

Sassen, K. and Dodd, G. C.: Lidar crossover function and misalignment effects, Appl. Opt., 21, 3162–3165, https://doi.org/10.1364/AO.21.003162, 1982.

Stelmaszczyk, K., Dell'Aglio, M., Chudzyński, S., Stacewicz, T., and Wöste, L.: Analytical function for lidar geometrical compression form-factor calculations, Appl. Opt., 44, 1323–1331, https://doi.org/10.1364/AO.44.001323, 2005.

Tomine, K., Hirayama, C., Michimoto, K., and Takeuchi, N.: Experimental determination of the crossover function in the laser radar equation for days with a light mist, Appl. Opt., 28, 2194, https://doi.org/10.1364/AO.28.002194, 1989.

Wandinger, U. and Ansmann, A.: Experimental determination of the lidar overlap profile with Raman lidar, Appl. Opt., 41, 2002.

Zenteno-Hernández, J. A., Comerón, A., Rodríguez-Gómez, A., Muñoz-Porcar, C., D'amico, G., and Sicard, M.: A comparative analysis of aerosol optical coefficients and their associated errors retrieved from pure-rotational and vibro-rotational raman lidar signals, Sensors (Switzerland), 21, 1–21, https://doi.org/10.3390/S21041277, 2021.